

23rd International Conference on Material Forming (ESAFORM 2020)

Unravelling Anisotropy Evolution during Spiral Pipe Forming: a Multiscale Approach

Matthias Bönisch^{a,*}, Albert Van Bael^a, Marc Seefeldt^a, Pere Barriobero-Vila^b,
Guillermo Requena^{b,c}, Nuria Sanchez^d, Steven Cooreman^d

^a*KU Leuven, Department of Materials Engineering, Kasteelpark Arenberg 44, box 2450, 3001 Leuven, Belgium*^b*German Aerospace Center (DLR), Institute of Materials Research, Linder Höhe, 51147 Cologne, Germany*^c*RWTH-Aachen, Metallic Structures and Materials for Aerospace Engineering, 52062 Aachen, Germany*^d*ArcelorMittal Global R&D Gent, OCAS NV, Pres. J. F. Kennedylaan 3, 9060 Zelzate, Belgium*

* Corresponding author. Tel.: +32 16 32 25 82. E-mail address: matthias.bonisch@kuleuven.be

Abstract

Spiral forming of bainitic steel coils into large diameter pipes involves a complex deformation history with several strain path changes. These lead to mechanical properties on pipe which are macroscopically different compared to coil. A detailed understanding of the property evolution during spiral pipe forming is crucial to tailor the coil material and to ensure safe pipe operation. However, it has proven difficult to correctly reproduce the anisotropic strength evolution during pipe forming with available phenomenological hardening models. Unravelling the factors contributing to macroscopic anisotropy is inherently a multi-scale problem due to the complex microstructures exhibited by modern bainitic linepipe steels. They promote a large Bauschinger effect, aside from cross loading-effects and more or less pronounced Lüders banding. Here, we present selected experimental and numerical results related to our efforts to predict the mechanical properties of bainitic steel pipes manufactured from hot rolled coils. Across the scales, we consider sources for anisotropy, such as residual stresses, crystallographic texture and grain substructure. A dislocation-based crystal plasticity model incorporated into a computationally efficient hierarchical multi-scale forming simulation is employed to predict texture and strength changes.

© 2020 The Authors. Published by Elsevier Ltd.

This is an open access article under the CC BY-NC-ND license (<https://creativecommons.org/licenses/by-nc-nd/4.0/>)

Peer-review under responsibility of the scientific committee of the 23rd International Conference on Material Forming.

Keywords: Residual stress; Texture; Bending; Dislocation substructure; Bauschinger effect; Synchrotron

1. Predicting mechanical behavior of spirally-welded high-strength low-alloy (HSLA) pipes

HSLA steel coils are used worldwide for the construction of long-distance, high-pressure gas and oil pipelines from large diameter spirally welded pipes. However, spirally-welded pipes are currently not fully exploited because of their anisotropic mechanical properties and reduced strength after pipe forming [1].

Understanding pipe anisotropy, strength evolution during forming and pipe failure mechanisms including plastic collapse and fracture is crucial to ensure safety and integrity of pipelines at high operating pressure and in environments subject to soil movement.

Relying on microalloying and tailored processing the utilized HSLA steels achieve unique combination of strength, toughness, weldability, chemical resistance and fatigue life [2]. However, the manufacturing process inevitably introduces mechanical anisotropy into the final pipe. The longitudinal direction of the spiral-welded pipe is rotated 40°–60° away from the rolling direction (RD) of the coil (figures 1a and 1b). As a result, the principal anisotropy axes are rotated relative to both the pipe principal axes (i.e. longitudinal and hoop) and the coil principal axes [3]. The material anisotropy manifests itself in variations in yield strength, tensile strength and toughness. For instance, a variation of the in-plane yield strength of some 10 MPa is observed on coil and on pipe [3–5] at a yield strength level of

2351-9789 © 2020 The Authors. Published by Elsevier Ltd.

This is an open access article under the CC BY-NC-ND license (<https://creativecommons.org/licenses/by-nc-nd/4.0/>)

Peer-review under responsibility of the scientific committee of the 23rd International Conference on Material Forming.

10.1016/j.promfg.2020.04.310

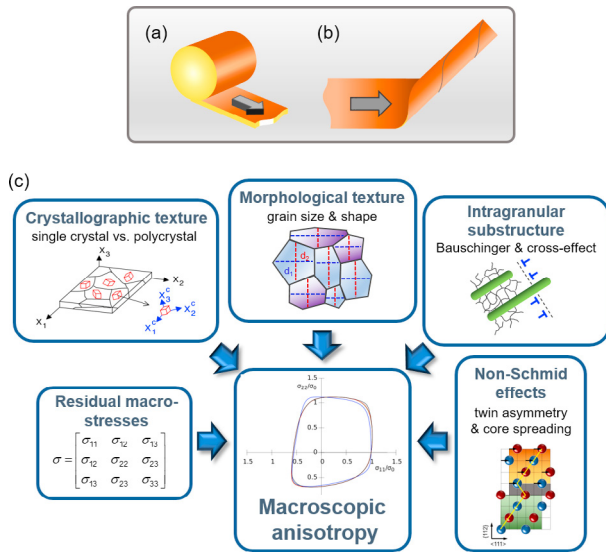


Fig. 1. The two major deformation steps in spiral pipe forming starting from coil: (a) decoiling and (b) spiral forming. (c) Sources of macroscopic mechanical anisotropy.

485–635 MPa for X70 linepipe grades [6]. In general, compared with its average value the yield strength on coil is increased along transverse direction (TD) and decreased along 30 to 45° with respect to RD [4]. In addition to yield strength, work hardening depends on the loading direction, too [3].

Simulating the entire forming process in order to predict the pipe properties from those on coil is a demanding task. A recent study, in which each spiral forming step was simulated via continuum level finite element (FE) models, concluded that the FE simulations allow predicting the properties along TD of the pipe but significantly underestimate the properties along the other directions [1]. This discrepancy was ascribed to the constitutive model used, which considered isotropic and kinematic hardening but did not allow for anisotropic hardening. A subsequent study demonstrated the clear benefit of including a phenomenological distortional (i.e. anisotropic) hardening law into the strength evolution [7].

Despite these progresses with phenomenological hardening models, the challenge lies in accounting appropriately for all relevant sources of anisotropy in a physical manner. Thereby not only properties of the final pipe could be predicted with superior accuracy but, what is more, such models could be used to reversely engineer microstructures for specific property profiles.

1.1. Sources of mechanical anisotropy

Here, we suggest 5 sources for macroscopic mechanical anisotropy (figure 1c):

- macroscopic residual stress (type I)
- crystallographic texture
- morphological texture
- dislocation substructure
- non-Schmid effects

While the present context is pipeline steels, these contributions are of relevance for any thermomechanically processed structural component. Below, we describe each contribution in relation to pipe forming.

1.2. Macroscopic residual stress

Repeated bending operations as they occur in forming a steel strip into a coil and into a pipe inevitably lead to internal residual stresses. A recent study suggested that the residual stresses in linepipe are more characteristic for the manufacturing process than for the specifics of the pipe, like its geometry (diameter and wall thickness) and steel grade [8]. A major driving factor for the development of residual stresses in pipe forming is the non-uniform deformation due to bending causing through-thickness strain and stress gradients [9]. This leads to a tensile plastic strain on the outside and compressive plastic strain on the inside of the bent plate. The associated elastic internal stresses can be of the same or of opposite sign as the plastic strain depending on whether springback is allowed. So far, it has been largely acknowledged that residual stress influences the susceptibility to stress corrosion, fatigue cracking and impact toughness of HSLA pipes [10, 11]. Much attention has been paid to residual stresses around weld joints [9, 12]. However, systematic investigations on how the through-thickness distribution of residual stress evolves during spiral pipe forming and on how the stress profile influences pipe anisotropy are missing.

1.3. Crystallographic texture

Crystallographic texture, describing the orientation distribution of crystallites in a polycrystalline material, undoubtedly affects mechanical (an)isotropy. Firstly, the thermomechanical processing steps, such as hot rolling, recrystallization and phase transformation, clearly impart crystallographic texture to the coils from which pipes are manufactured. Secondly, the pipe forming process starting from coil could modify this crystallographic texture - like every forming process does. However, the extent to which crystallographic texture determines coil and pipe anisotropy is not fully clear. It has been recognized that mechanical anisotropy is the result of complex combination of microstructure with crystallographic texture [13]. In addition, it has been stipulated that crystallographic texture plays the greatest role in determining strength anisotropy in grades above X70 [14, 15]. In low grades, such as X52, on the other hand, crystal plasticity simulations suggested that crystallographic texture is of minor relevance and sources related to the microstructure, such as grain shape and distribution of inclusions, play a primary role [4].

1.4. Morphological texture

Modern pipeline grades are often predominantly bainitic with polygonal, quasi-polygonal, acicular and bainitic ferrite. Minor fractions of austenite, martensite and non-metallic inclusions like carbides, nitrides, oxides, sulphides can add further complexity to the spatial and orientation distribution of

the phase- and grain-boundary network [16–18].

The shape and alignment of grains in a polycrystalline microstructure is commonly referred to as morphological texture. Being a direct result of thermomechanical processing and forming operations it has been suggested as an important source of mechanical anisotropy in pipeline steel [5, 14]. Especially, when the microstructural anisotropy is large other sources of anisotropy are often of secondary importance. This is observed in the cases of highly elongated or flattened grains, a non-uniform distribution of hard particles or pearlite due to banding because of segregation of solutes during solidification [14].

1.5. Dislocation substructure

Plastic deformation of bcc ferrite leads to an intragranular substructure consisting of dislocation cells, cell blocks and cell block boundaries (CBBs), whose spatial arrangement and density depend on the deformation history [19, 20]. While the dislocation cells, filling the volume of individual cell blocks, are randomly oriented and lead to isotropic hardening, the CBBs, which separate cell blocks, form on the most active slip planes only. They limit the mean free path of dislocations on less active slip planes, and their non-random nature leads to the grain strength and hardening to become anisotropic, similar to the effect of grain boundaries for non-spherical grain shapes [21]. The importance of the dislocation substructure for the accurate modelling of mechanical anisotropy in the presence of strain-path changes has been recognized and receives increasing attention. Specifically, Bauschinger and cross-effects, which are pronounced in pipeline steels [7, 18], are related to the dislocation substructure and need to be accounted for appropriately [22, 23].

1.6. Non-Schmid effects

While all previous anisotropy sources relate to the microstructural configurations at the level of polycrystals and of single grains, it has been suggested that the atomic lattice itself could be a source of mechanical anisotropy. Since long bcc single and polycrystals, including Fe, are known to exhibit pronounced non-Schmid behavior leading to a strong tension-compression asymmetry [24–26]. The uni-directional nature of mechanical twinning is certainly one of the reasons. For bcc lattices it is for instance well established that such an asymmetry exists on the $\{112\}\langle 111 \rangle$ twin-anti twin systems. Furthermore, even for a random texture the non-planar spreading of $1/2\langle 111 \rangle$ screw dislocation cores can lead to a pronounced tension-compression asymmetry [26]. Moreover, recent studies reported ferrite transformation twins in API X grades [16, 27], which could have a pronounced effect on the directionality of the mechanical response [28].

While it is acknowledged that the non-Schmid behavior weakens with increasing temperature, for Fe it may lead to an increase of the room temperature compressive yield strength by 50% relative to that in tension [25]. To this date, the influence of non-Schmid effects (i.e. twin-anti twin asymmetry and dislocation core spreading) and of transformation twins on the macroscopic anisotropy of pipeline steel is unclear.

1.7. The focus of the current study

In the present study, we concentrate on 3 out of the 5 anisotropy sources discussed above: (i) macroscopic residual stress, (ii) crystallographic texture and (iii) the intragranular dislocation substructure. To this end, we examine two bainitic API grade X70 steels of different thickness (16 mm, 22.7 mm) in terms of crystallographic texture and residual stress after hot rolling and coiling. We experimentally determine detailed thickness residual stress profiles for both materials using high-energy X-ray diffraction (HEXRD). Using the hierarchical multi-scale forming simulation (HMS) framework developed at KU Leuven [29], we simulate the elementary forward-reverse bending process occurring during pipe forming to assess associated texture changes. Aiming to include intragranular contributions due to dislocation substructures in the flow stress predictions, a calibration routine for the Peeters substructural hardening model [20] has been developed. To fit stress-strain data from strain-path change tests we implemented a Bayesian algorithm.

2. Results and Discussion

2.1. Coil residual macro-stress

Residual strain was measured on the coils using HEXRD and converted to the corresponding stress. The high penetration depth of synchrotron X-rays compared to laboratory X-ray sources allows the use of bulk samples and limits stress relaxation occurring during sample extraction. To this end, samples of 4–5 mm constant thickness were cut from the coils perpendicular to RD and TD by electrical discharge machining. This thickness provided adequate transparency and a reasonably large diffracting volume for HEXRD, which was performed at the beamline P07 at DESY, Hamburg, in transmission mode using a beam energy of 100keV. The beam cross-section was adjusted to $0.1 \times 0.1 \mu\text{m}^2$ to obtain enough spatial resolution. Samples were then scanned stepwise along the normal direction (ND) with the X-ray beam parallel to either RD or TD (see figure 2). Every 0.2 mm (X70-16mm) and 0.3 mm (X70-22.7mm) ring diffraction patterns were recorded on a 2-dimensional area detector (Perkin Elmer). A triaxial elastic strain state was fitted to each diffraction pattern pair along ND via the $\sin^2\psi$ method, utilizing Maud (maud.radiographema.eu) [30]. The instrumental parameters of the HEXRD setup were calibrated using a LaB_6 powder standard. Due to the weak crystallographic texture of the coil (see section 2.2), elastic isotropy (Young's modulus $E = 210$ GPa, Poisson's ratio $\nu = 0.3$) was assumed for derivation of stresses from strains. Stress determined in this way corresponds to the average stress across many grains, commonly referred to as type I residual stress. The resulting thickness profiles for stress, strain and lattice parameter are shown in figure 2; refinement uncertainties are smaller than the markers used for plotting. The profiles reveal large

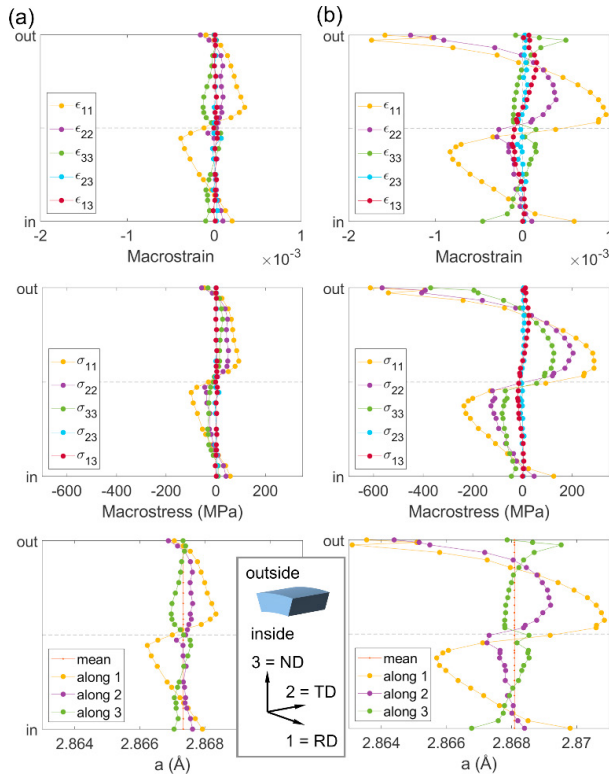


Fig. 2. Residual strain, stress and lattice parameter profiles measured on coil for (a) X70-16mm and (b) X70-22.7mm. The reference frame used is indicated in (a) at the bottom.

residual stresses in both materials. They follow S-curves, characteristic for a bending operation followed by elastic springback where along RD a normal compressive residual stress develops on the stretched (outer) surface and a tensile residual stress at the compressed (inner) surface. Normal stresses are largest along RD, followed by TD and ND. For the 16mm coil, the RD normal stress reaches ± 100 MPa close to mid-thickness, while for the 22.7mm coil the RD component reaches -230 MPa and 290 MPa close to mid-thickness and climbs to a very large value of -600 MPa at the coil outside. Compared to the normal components, shear stresses are relatively small, but still reach +25 MPa in case of σ_{13} for X70-22.7mm. Since for the outermost data points close to the coil in- and outside the beam was positioned $\sim 200\mu\text{m}$ away from the respective surface towards mid-thickness, the ND components exhibit finite values at these positions.

These results clearly show that among hot rolling and coiling, the latter dominates the residual stress development, at least in the 16mm thick coil. In case of the 22.7mm variant, the measured stresses indicate influences of both rolling and coiling: while pure bending gives rise to stress distributions symmetric about mid-thickness in terms of magnitude, the stresses close to coil out- and inside are asymmetric, shifted to the compressive regime (figure 2b). This asymmetry reveals a superposition of the effect of bending (i.e. coiling) with that of rolling, which is known to generate compressive stress at the plate surfaces [31]. Notably, in the 22.7mm variant the RD component on the outer surface approaches the material flow

stress and considerably larger residual stresses develop by coiling compared to X70-16mm. As a result of the stress variations along the thickness, different in-plane layers of the coil are anticipated to yield at different imposed stresses. E.g., when loaded in tension along RD, layers of positive (tensile) RD residual stress component will reach the material flow stress first and commence yielding. Those layers of negative (compressive) residual stress along RD will start plastic yielding last. The ensuing gradual, i.e. layer-by-layer, plastification is projected to affect the elastoplastic transition considerably: a flat residual stress profile, corresponding to a narrow yield stress distribution (such as in fig. 2a), will give rise to a sharp macroscopic yield point, whereas a 'mountainous' residual stress profile (such as in fig. 2b), corresponding to a wide yield stress distribution, will lead to an extended elastoplastic transition. Furthermore, depending on the magnitude of the residual stress profile the external stress required to reach the material flow stress will be larger (small RS magnitude) or smaller (large RS magnitude). Undoubtedly, these factors render the macroscopic yielding behavior of the plate anisotropic. In addition, care must be taken when extracting mechanical test specimens, as their loading response will be affected not only by their in-plane orientation but also by their dimensions and position along the plate thickness.

2.2. Coil crystallographic texture

X-ray pole figure measurements were performed to characterize the crystallographic texture of the coils prior to pipe forming. To this end, a Bruker D8 Advance goniometer with a Cu tube and secondary beam monochromator was used. Based on 4 ferrite pole figures ($\{111\}$, $\{200\}$, $\{220\}$, $\{311\}$) the pertaining orientation distribution functions (ODFs) displayed in figures 3 and 4 were constructed using MTM-FHM [32]. X70-22.7mm shows rolling, recrystallization and transformation texture components with partial α - and γ -fibers and a weak β -fiber, all with high homogeneity across the thickness. In X70-16mm the α -fiber is weak, and the γ -fiber is largely absent. The bcc β -fiber, characteristic for $\gamma \rightarrow \alpha$ transformation textures, dominates and exhibits a clear gradient towards the outside of the coil.

2.3. Crystallographic texture evolution

Crystallographic texture is a major factor defining mechanical anisotropy in metals and alloys. It is inevitably linked to plastic deformation, proceeding via dislocation slip at the lattice level. To assess texture evolution during pipe forming and its effect on macroscopic anisotropy we simulated plane strain bending, the fundamental deformation mode occurring in pipe forming. In reality, one starts from a curved coil section, which is flattened and then formed into a pipe (figures 1a and 1b). This process involves forward and reverse bending. We created an explicit FE model, shown in fig. 5a, with the bending axis parallel to TD of the coil and the global Z-axis. Due to mirror symmetry of the bending geometry with respect to the RD plane, the FE model is

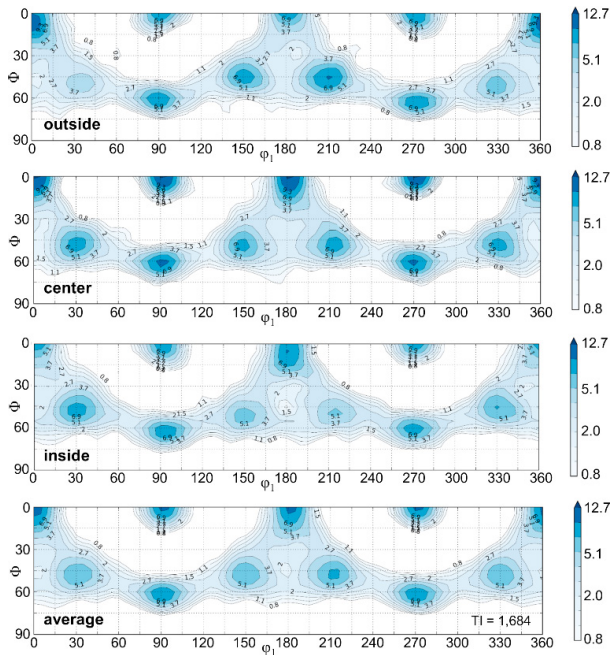


Fig. 3. Measured $\varphi_2 = 45^\circ$ ODF sections for X70-22.7mm coil.

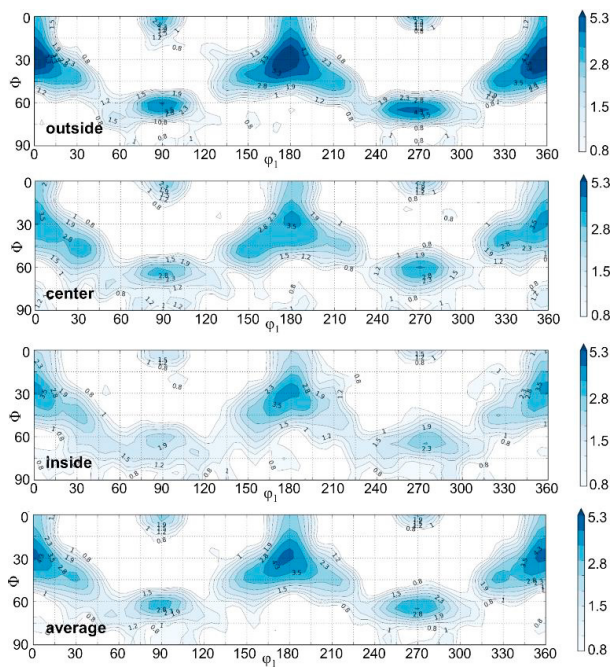


Fig. 4. Measured $\varphi_2 = 45^\circ$ ODF sections for X70-16mm coil.

reduced to one half of the modelling space.

Texture evolution in each integration point of the FE model was predicted using HMS coupled to the ALAMEL relaxed-constraints crystal plasticity model [29, 33], starting from the measured average through-thickness textures in figures 3 and 4. The hierarchical multi-scale framework, in its configuration utilized here, considers 2 different length scales:

- macroscopic, corresponding to the continuum level FE model of the pipe section
- mesoscopic, corresponding to a single FE integration point (IP) consisting of a few 1000 grains interacting pair-wise

Each IP holds essential internal state variables describing the current local material properties, including texture and the yield surface represented by the Facet plastic potential [34]. By means of the ALAMEL model slip activity, texture change resulting from grain rotation, as well as the homogenized stress are calculated throughout each IP in response to the imposed plastic strain rate. To be able to study the influence of crystallographic texture evolution independent from other sources of mechanical anisotropy, texture was the only anisotropy source considered in these simulations. The mechanical anisotropy of an IP was regularly updated from the texture through virtual experiments using ALAMEL. Slip was allowed on the 24 systems of types $\langle 111 \rangle \{110\}$ and $\langle 111 \rangle \{11\bar{2}\}$, with identical critical resolved shear stress (CRSS) on all systems. Hardening was described by an isotropic Swift law, calibrated on full thickness tensile tests along the coils' TD and internally translated to the matching shear stress vs. shear strain relationship.

Figures 5 - 7 illustrate the simulation results for cyclic bending (forward bending followed by reverse bending) of X70-22.7mm through a curvature typical for decoiling and spiral pipe forming. While the simulations predicted considerable residual stresses of several 100 MPa (figure 5),

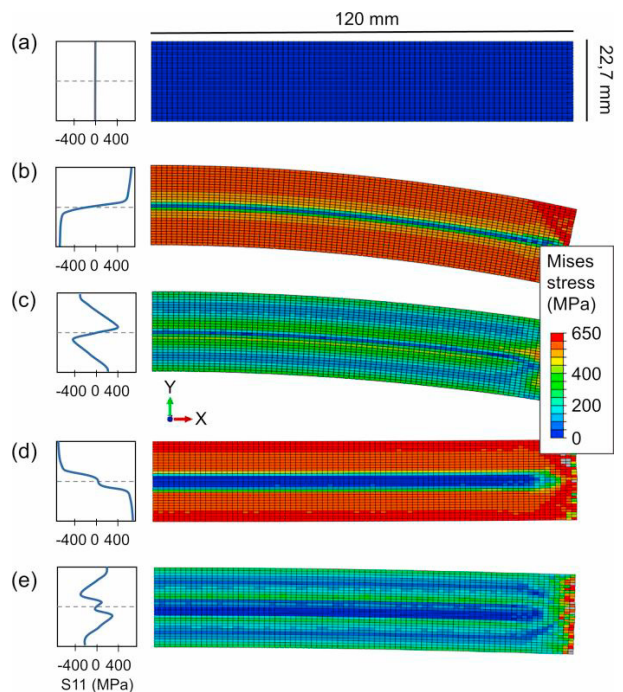


Fig. 5. Stress evolution during cyclic bending and springback HMS simulation for X70-22.7mm: (a) initial, (b) maximum forward bending moment of 84 Nm, (c) springback after forward bending, (d) maximum reverse bending moment of -84 Nm, (e) springback after reverse bending. The bending axis is Z. Profiles of the normal stress component along X (S11) and maps of the von Mises stress are shown on the left and right, respectively.

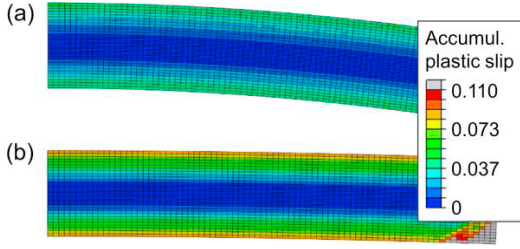


Fig. 6. Accumulated plastic slip after (a) forward bending and springback, and (b) after reverse bending and springback.

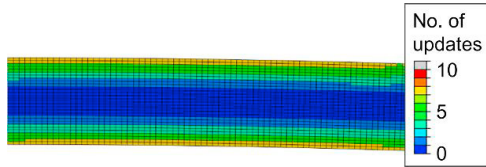


Fig. 7. Number of property updates after cyclic bending and springback.

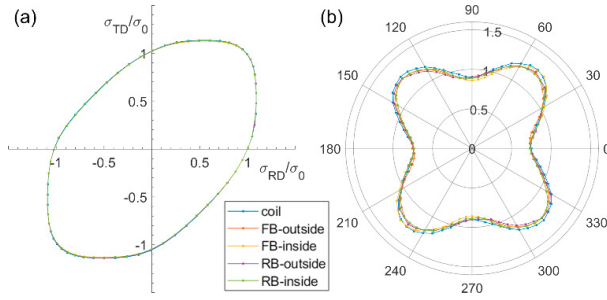


Fig. 8. (a) $\sigma_{ND} = 0$ yield locus sections and (b) in-plane r -value anisotropy for monotonic forward (FB) and reverse bending (RB) at the out- and inside of the X70-22.7mm bent plate. Outside and inside correspond to the top left and bottom left elements of the FE model in figure 5. The polar angle in (b) is given relative to RD.

macroscopic strains are small ($< 3\%$ at the plate surface along RD for monotonic bending). After forward and reverse bending the accumulated plastic slip amounts to $\sim 9\%$ (figure 6). At the plate surface, texture was updated 7 times (figure 7). The resulting ODF changes are weak (between $+0.5$ and -1) and are not shown here for brevity reasons. On both plate surfaces bending operations reduce the texture sharpness, by up to -1 at the inner surface. Simulations with the full-constraints Taylor crystal plasticity model and 48 instead of 24 slip systems (by permitting slip on $\langle 111 \rangle \{12\text{-}3\}$) altered the texture evolution only marginally. Adding the reverse bending step after forward bending slightly inverted the texture changes by forward bending: those components weakened strongest by forward bending were again sharpened.

Macroscopically, plastic anisotropy is largely unaffected by these texture alterations, as illustrated by the yield locus sections and r -value distributions in figure 8. The initial yield locus is modified by $< 1\%$ by forward and reverse bending as far as its shape and its link to crystallographic texture is concerned. The yield surface sections in figure 8a thus come to lie on top of each other. r -values change by $< 5\%$ (figure 8b). The observed negligible effect of texture evolution on

anisotropy can be ascribed to the relatively low plastic deformation involved in pipe forming. In the simulations discussed here, the macroscopic logarithmic strain along RD was always below 0.03 and texture changes accordingly minimal. A similar conclusion is suggested by a recent experimental report on microtexture evolution during pipe forming [35].

Controlling the contribution of crystallographic texture to pipe anisotropy is therefore equivalent to controlling the crystallographic texture of the coil. This could be achieved by tailoring of the thermomechanical rolling protocols for coil production from steel slabs.

2.4. Substructural dislocation hardening

The intragranular dislocation substructure is a major source for macroscopic mechanical anisotropy, manifesting itself in reverse- (Bauschinger) and cross-effects when the strain-path changes. Here, we show an attempt to calibrate the Peeters substructural hardening model [20] to cyclic Bauschinger tests coupled to the relaxed-constraints ALAMEL code [33], incorporates dislocation ensembles into a polycrystal plasticity model, in order to predict flow stress variations upon strain path changes. It schematizes the inhomogeneous intragranular substructure into dislocation cells, CBBs and dislocation pile-ups at CBBs. Further, it associates each of these features with a dislocation density, namely ρ (dislocation cells), ρ_i^{wd} (CBB on plane i of the 6 $\{110\}$ planes) and ρ_i^{wp} (net dislocation pile-up at CBB i). While the CBBs are responsible for latent hardening leading to cross-effects, the pile-ups polarize the CBBs leading to reverse (Bauschinger) effects upon strain reversal.

The CRSS τ_s^c on a slip system s is modelled as the sum of 4 contributions:

$$\tau_s^c = \tau_0 + (1-f)\tau^{CB} + f \sum_{i=1}^6 (\tau_{is}^{wp} + \tau_{is}^{wd}) \quad (1)$$

where

$$\tau^{CB} = \alpha G b \sqrt{\rho}$$

$$\tau_{is}^{wp} = \alpha G b \left| \mathbf{u}_s^b \cdot \mathbf{u}_i^w \right| \text{sign}(\rho_i^{wp}) \sqrt{|\rho_i^{wp}|}$$

$$\tau_{is}^{wd} = \alpha G b \left| \mathbf{u}_s^b \cdot \mathbf{u}_i^w \right| \sqrt{\rho_i^{wd}}$$

τ_0 includes contributions independent of the dislocation substructure, among them the Peierls-Nabarro stress and initial grain size. Isotropic hardening due to cell formation and accumulation of statistically stored dislocations is represented by τ^{CB} . α , G and b are the dislocation interaction strength, shear modulus, and Burgers vector, deemed constant material parameters in the present context. While τ_{is}^{wp} encodes the slip direction-dependent impact of dislocation pile-ups at CBBs giving rise to the Bauschinger effect, τ_{is}^{wd} describes latent

hardening giving rise to the cross effect. $\mathbf{u}_s^b \cdot \mathbf{u}_l^w$ is the scalar product of the slip direction with the normal to the CBB plane and modifies the slip resistance on all slip systems that are non-coplanar with the CBB. $\langle \cdot \rangle$ indicates the left-continuous Heaviside function centered at 0. It leads to an asymmetric slip resistance by allowing piled-up dislocations to move away from the CBB without resistance when a previously active slip system operates in the opposite sense. The total CRSS in equation 1 is obtained by assuming a linear rule of mixture for contributions from dislocation cells and CBBs using the volume fraction f of CBBs as weighting factor. 11 model parameters together with the slip activity as a function of crystallite orientation control the dislocation density evolution.

To calibrate the Peeters model based on measured flow curves we developed a fitting routine in Python. This minimizes a cost function (in the present case the least-squares residual $R(\bar{p})$ between simulated and measured flow curves) where \bar{p} denotes a location in parameter space (i.e. a set of model parameter values). The large parameter space combined with the non-analytical relationship between model parameters and resulting stress-strain curves rule out simple search procedures. For instance, a basic grid search in parameters space would take prohibitively long. Therefore, a gradient-free Bayesian optimization algorithm, adapted to the current task, was implemented using the *hyperopt* package [36]. Individual simulation runs for the selected parameter sets \bar{p} were driven by the virtual experimentation framework (VEF) developed at KU Leuven [37]. The calibration procedure operates in the following sequence:

- choose a location \bar{p}_n in parameter space
- call VEF to simulate the pertaining flow curve(s)
- calculate the cost function from measured and simulated stresses
- call the Bayesian algorithm to determine most promising new parameter set \bar{p}_{n+1} and start again from step ii

Figure 9 shows the trial calibration for Bauschinger tests along RD of X70-16mm coil. The experimental stress-strain curve (figure 9a) demonstrates large flow stress differentials of ~250 MPa on reverse loading, independent of the sign of the strain path change (tension-compression vs. compression-tension). As illustrated in figure 9b, the large transients occurring after load reversal cannot be satisfactorily reproduced by the Peeters model. Exploration of the parameter space showed that the Peeters model could in principle produce Bauschinger stress differentials larger than several 10 MPa, yet at the cost of unphysical parameter values, such as an exaggerated volume fraction of CBBs and over-amplified storage rates for CBB and polarizing dislocation densities.

These results strongly indicate that sources other than the dislocation substructure contribute to the large Bauschinger effect in this pipeline steel. The Bauschinger effect can be commonly rationalized by back stresses created by the piling-up of dislocations of the same sign at obstacles [38, 39], such

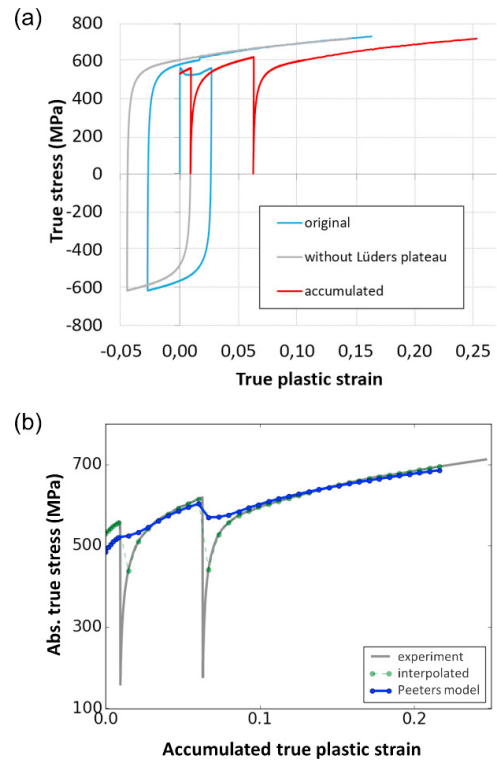


Fig. 9. (a) Cyclic Bauschinger test for X70-16mm along RD of the coil. (b) Comparison of experimental and the best fit flow curve simulated using the Peeters model.

as CBBs, grain boundaries or inclusions. During forward deformation, back-stresses are built up at the slip obstacles and during reverse deformation they assist the backward movement of the dislocations away from the obstacle. In the Peeters model, the Bauschinger effect is accounted for purely through the dislocation substructure, i.e. by the reversible accumulation of dislocations at CBBs. That said, interactions with grain boundaries and/or inclusions are not included in the model. These can be, however, substantial in pipeline steels [17]. Figure 9b suggests that grain boundaries and/or inclusions play an important role in explaining the flow stress transients observed upon strain reversals. We therefore conclude here that a realistic dislocation-based model for the Bauschinger effect in pipeline steel needs to include pile-up formation at grain boundaries and/or inclusions.

2.5. Conclusions

The present investigation clearly evidences the multifaceted nature of mechanical anisotropy in modern pipeline steels. Substantial residual macro-stress was found in X70 coils of different thicknesses. The elemental bending operations of pipe forming hardly change the crystallographic texture. As a result, crystallographic texture-induced plastic anisotropy is virtually unaffected by pipe forming. Anisotropy sources other than crystallographic texture, such as residual stresses or reversible dislocation-obstacle interactions, are responsible for the strength evolution observed during pipe forming. Future

computational studies of pipe forming should focus on the following 2 aspects:

- Including macroscopic internal stress (residual stress type I) originating from the coil production.
- Extending dislocation-based Bauschinger effect models by dislocation-grain boundary and dislocation-inclusion interactions.

This work furthermore demonstrates the need for an integrated approach to unravel the superimposed effects of anisotropy sources in HSLA pipes.

Acknowledgments

The Deutsches Elektronen-Synchrotron (DESY) is acknowledged for the provision of synchrotron radiation facilities in the framework of proposal I-20180384.

References

- [1] Cooreman S, Van Hoecke D, Liebeherr M, Thibaux P, and Yamaguti Enderlin M. Experimental and numerical study on the evolution of mechanical properties during spiral pipe forming. In: 11th Int. Pipeline Conf. (IPC2018). 2016. Calgary, Alberta, Canada; ASME
- [2] Cochrane RC. Phase transformations in microalloyed high strength low alloy (HSLA) steels. In: Phase transformations in steels, E. Pereloma and D.V. Edmonds, Editors. 2012, Woodhead Publishing. p. 153-212.
- [3] Iob F, Cortese L, Di Schino A, and Coppola T. Influence of mechanical anisotropy on micro-voids and ductile fracture onset and evolution in high-strength low alloyed steels. *Metals* 2019;9:224.
- [4] Sanchez N, Van Hoecke D, and Liebeherr M. Mechanical anisotropy of hot rolled line pipe steel coil. In: 9th Int. Pipeline Conf. (IPC2012). 2012. Calgary, Alberta, Canada; ASME
- [5] Gervasyev A, Petrov R, Pyshmintsev I, Struin A, Leis B, and Asme. Mechanical properties anisotropy in X80 line pipes. In: 11th Int. Pipeline Conf. (IPC2016). 2016. Calgary, Alberta, Canada; ASME
- [6] Petroleum and natural gas industries-steel pipe for pipeline transportation systems. 2007, International Standardisation Organisation.
- [7] Cooreman S, Thibaux P, and Liebeherr M. Prediction of mechanical properties on large diameter welded pipes through advanced constitutive modelling. In: NUMISHEET. 2018. Tokio, Japan; J. of Physics: IOP Conf. Series 1063:012043.
- [8] Lothhammer LR, Viotti MR, Veiga CLN, and Albertazzi A. Experimental evaluation of residual stresses in pipes manufactured by UOE and ERW processes. *Exp Mech* 2017;57:287-296.
- [9] Law M, Prask H, Luzin V, and Gnaeupel-Herold T. Residual stress measurements in coil, linepipe and girth welded pipe. *Mater Sci Eng A* 2006;437:60-63.
- [10] Mandal A, Syed B, Bhandari KK, Bhattacharya B, Deb A, Singh SB, and Chakrabarti D. Cold-bending of linepipe steel plate to pipe, detrimental or beneficial? *Mater Sci Eng A* 2019;746:58-72.
- [11] Lavigne O, Kotousov A, and Luzin V. Microstructural, mechanical, texture and residual stress characterizations of X52 pipeline steel. *Metals* 2017;7:306.
- [12] Mirzaee-Sisan A and Wu G. Residual stress in pipeline girth welds - a review of recent data and modelling. *Int J Pres Ves Pip* 2019;169:142-152.
- [13] Tankoua F, Crépin J, Thibaux P, Cooreman S, and Gourgues-Lorenzon AF. Quantification and microstructural origin of the anisotropic nature of the sensitivity to brittle cleavage fracture propagation for hot-rolled pipeline steels. *Int J Frac* 2018;212:143-166.
- [14] Joo MS, Suh DW, and Bhadeshia HKDH. Mechanical anisotropy in steels for pipelines. *ISIJ Int* 2013;53:1305-1314.
- [15] Mouriño NS, Petrov R, Bae J-H, Kim K, and Kestens LaI. Texture dependent mechanical anisotropy of X80 pipeline steel. *Adv Eng Mater* 2010;12:973-980.
- [16] Shanmugam S, Misra RDK, Hartmann J, and Jansto SG. Microstructure of high strength niobium-containing pipeline steel. *Mater Sci Eng A* 2006;441:215-229.
- [17] Carretero Olalla V, Bliznuk V, Sanchez N, Thibaux P, Kestens LaI, and Petrov RH. Analysis of the strengthening mechanisms in pipeline steels as a function of the hot rolling parameters. *Mater Sci Eng A* 2014;604:46-56.
- [18] Kostryzhev AG, Strangwood M, and Davis CL. Bauschinger effect in Nb and V alloyed line-pipe steels. *Ironmak Steelmak* 2009;36:186-192.
- [19] Peeters B, Bacroix B, Teodosiu C, Van Houtte P, and Aernoudt E. Work-hardening/softening behaviour of b.c.c. polycrystals during changing strain: Part II. TEM observations of dislocation sheets in an IF steel during two-stage strain paths and their representation in terms of dislocation densities. *Acta Mater* 2001;49:1621-1632.
- [20] Peeters B, Seefeldt M, Teodosiu C, Kalidindi SR, Van Houtte P, and Aernoudt E. Work-hardening/softening behaviour of b.c.c. polycrystals during changing strain paths: Part I. An integrated model based on substructure and texture evolution, and its prediction of the stress-strain behaviour of an IF steel during two-stage strain paths. *Acta Mater* 2001;49:1607-1619.
- [21] Kestens L, Sanchez N, Decroos K, and Petrov RH. Yield strength anisotropy of steel sheet induced by grain shape and crystal anisotropy. In: Textures of Materials (ICOTOM 16). 2012. Mumbai, India; Mater. Sci. Forum 702-703:419-426.
- [22] Kitayama K, Tomé CN, Rauch EF, Gracio JJ, and Barlat F. A crystallographic dislocation model for describing hardening of polycrystals during strain path changes. Application to low carbon steels. *Int J Plast* 2013;46:54-69.
- [23] Eyckens P, Van Bael A, Moerman J, Vegter H, and Van Houtte P. Prediction of transient hardening after strain path change by a multi-scale crystal plasticity model with anisotropic grain substructure. *Procedia Eng* 2014;81:1318-1323.
- [24] Chowdhury P and Sehitoglu H. Atomistic energetics and critical twinning stress prediction in face and body centered cubic metals: Recent progress. *J Eng Mater Technol* 2018;140.
- [25] Patra A, Zhu T, and McDowell DL. Constitutive equations for modeling non-schmid effects in single crystal bcc-Fe at low and ambient temperatures. *Int J Plast* 2014;59:1-14.
- [26] Vitek V, Mrovec M, Gröger R, Bassani JL, Racherla V, and Yin L. Effects of non-glide stresses on the plastic flow of single and polycrystals of molybdenum. *Mater Sci Eng A* 2004;387-389:138-142.
- [27] Zhang J, Luo T, Wang X, Zhu Y, and Yu C. Formation mechanism of nanoscale transformation twinning in ultra-low-carbon high-strength pipeline steels. *J Mater Sci* 2019;54:14950-14960.
- [28] Sainath G and Choudhary BK. Deformation behaviour of body centered cubic iron nanopillars containing coherent twin boundaries. *Philos Mag* 2016;96:3502-3523.
- [29] Gawad J, Van Bael A, Eyckens P, Samaey G, Van Houtte P, and Roose D. Hierarchical multi-scale modeling of texture induced plastic anisotropy in sheet forming. *Comput Mater Sci* 2013;66:65-83.
- [30] Wenk H-R, Lutterotti L, Kaercher P, Kanitpanyacharoen W, Miyagi L, and Vasin R. Rietveld texture analysis from synchrotron diffraction images. II. Complex multiphase materials and diamond anvil cell experiments. *Powder Diffr* 2014;29:220-232.
- [31] Prime MB and Hill MR. Residual stress, stress relief, and inhomogeneity in aluminum plate. *Scripta Mater* 2002;46:77-82.
- [32] Van Houtte P. The MTM-FHM software system. Version 2000;2:1-76.
- [33] Van Houtte P, Li S, Seefeldt M, and Delannay L. Deformation texture prediction: From the Taylor model to the advanced Lamel model. *Int J Plast* 2005;21:589-624.
- [34] Van Houtte P, Yerra SK, and Van Bael A. The Facet method: A hierarchical multilevel modelling scheme for anisotropic convex plastic potentials. *Int J Plast* 2009;25:332-360.
- [35] Li J, Su L, Lu C, Li H, and Luo D. The evolution of microtexture of pipeline steel from strip to bare pipe to coated pipe. *Procedia Eng* 2017;207:1844-1849.
- [36] Bergstra J, Yamins D, and Cox DD. Making a science of model search: Hyperparameter optimization in hundreds of dimensions for vision architectures. In: 30th Int. Conf. on Machine Learning. 2013. Atlanta, GA, USA; J. Mach. Learn. Res. 28(1):115-123.
- [37] Gawad J, Banabic D, Van Bael A, Comsa DS, Gologanu M, Eyckens P, Van Houtte P, and Roose D. An evolving plane stress yield criterion based on crystal plasticity virtual experiments. *Int J Plast* 2015;75:141-169.
- [38] Bate PS and Wilson DV. Analysis of the Bauschinger effect. *Acta Metall* 1986;34:1097-1105.
- [39] Brown LM. Orowan's explanation of the Bauschinger effect. *Scr Metall* 1977;11:127-131.